NUKLEONIKA 2023;68(1):11–17
doi: 10.2478/nuka-2023-0002

ORIGINAL PAPER

sciendo

Investigation of low-temperature plasmas formed in low-density gases surrounding laser-produced plasmas

Mateusz Majszyk,
Andrzej Bartnik,
Wojciech Skrzeczanowski,
Tomasz Fok,
Łukasz Węgrzyński,
Mirosław Szczurek,
Henryk Fiedorowicz

Abstract. Low-temperature plasma production is possible as a result of photoionization using high-intensity extreme ultraviolet (EUV) and soft X-ray (SXR) pulses. Plasma of this type is also present in outer space, e.g., aurora borealis. It also occurs when high-velocity objects enter the atmosphere, during which period high temperatures can be produced locally by friction. Low-temperature plasma is also formed in an ambient gas surrounding the hot laser-produced plasma (LPP). In this work, a special system has been prepared for investigation of this type of plasma. The LPP was created inside a chamber filled with a gas under a low pressure, of the order of 1–50 mbar, by a laser pulse (3–9 J, 1–8 ns) focused onto a gas puff target. In such a case, the SXR/EUV radiation emitted from the LPP was partially absorbed in the low-density gas. In this case, high- and low-temperature plasmas (T_e ~100 eV and ~1 eV, respectively) were created locally in the chamber. Investigation of the EUV-induced plasmas was performed mainly using spectral methods in ultraviolet/visible (UV/VIS) light. The measurements were performed using an echelle spectrometer, and additionally, spatial–temporal measurements were performed using an optical streak camera. Spectral analysis was supported by the PGOPHER numerical code.

Keywords: Extreme ultraviolet (EUV) • Laser plasma • Low pressure • Photoionization • Plasma • Soft X-ray (SXR)

M. Majszyk✉, A. Bartnik, W. Skrzeczanowski, T. Fok, Ł. Węgrzyński, M. Szczurek, H. Fiedorowicz
Institute of Optoelectronics
Military University of Technology
Kaliskiego 2 St., 00-908 Warsaw, Poland
E-mail: mateusz.majszyk@wat.edu.pl

Received: 6 October 2022
Accepted: 5 December 2022

Introduction

The formation of chemical compounds or individual molecules is an indispensable element of nature. It is important to know what conditions are conducive to the formation of specific chemical compounds. In the case of plasma, this requires exceeding of the ionization, excitation, or dissociation energies. They are different for each element/molecule, and these energies usually start at a few electron volts. Various species are created in this manner. It can lead to the formation of new molecular species, not existing in the initial gaseous mixture. The molecular species can be stable or transient. Their formation requires suitable plasma conditions.

Such processes can be induced by extreme ultraviolet (EUV) or soft X-ray (SXR) radiation. In normal terrestrial conditions, we do not encounter this radiation. It stops in the upper parts of the atmosphere, ionizing its components. It can lead to the escape of particles from the planet's atmosphere or contribute to the molecular processes mentioned above. Similar processes may occur on other planets or moons with their own atmospheres [1, 2], especially taking into account the ubiquitous presence of this type of radiation in space, e.g., of stellar origin, including the Sun. The formation of

molecules under such conditions can lead to more complex structures, including the foundations of life [3]. Another phenomenon that can cause ionization of both interstellar dust and the atmosphere of the celestial body is the entry of a meteor into it [4].

Many laboratory solutions can be used to obtain atomic, ionic, or molecular processes. EUV or SXR radiation can be produced in various ways. One way to get a broad spectrum from X-rays to infrared (IR) is through synchrotron systems, but it is an expensive and complex setup; another is free electron lasers (FELs), and yet another is plasma source. Plasma sources include those based on high-power discharge-produced plasma (DPP) or laser-produced plasmas (LPPs).

In this work, the LPP source was used to generate radiation in the EUV/SXR range. Such solutions have been used many times to generate this type of radiation [5]. Owing to the use of a gas target by such a source, various gas mixtures, suitably prepared in advance, can be used. They can include simple molecular gases, e.g., nitrogen, and more complex mixtures of various gases, e.g., a mixture of krypton, sulfur, fluorine, and helium. This solution allows the observation of the formation of new particles as a result of the interaction of the used gases with radiation from the LPP source.

Experimental setup

The experimental system (Fig. 1) consists of a small vacuum chamber that can be filled with the investigated gas mixture under low pressure (1–50 mbar). The system shown in Fig. 1 can be divided into two parts: the first one designed for production of the LPPs, and the second one dedicated for the investigation of low-temperature plasmas formed around the LPP. The LPPs were formed using a neodymium-doped yttrium aluminum garnet (Nd:YAG) laser, which was focused onto a gas puff target. The target consists of an identical gas mixture that fills the chamber, but its density is much higher, close to the atmospheric density ($\sim 10^{19}$ m^{-3}). The second system allows for measurements of the ultraviolet/visible (UV/VIS) radiation emitted from plasmas produced by the LPP source. Measurements are carried out using an optical spectrometer and streak camera.

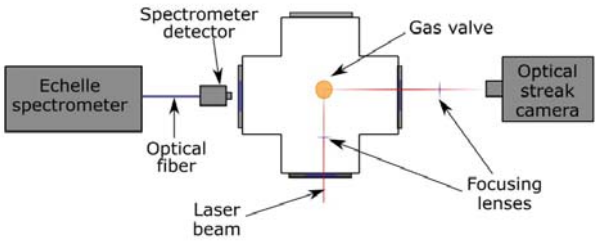

Fig. 1. Schematic view of the experimental system for time–space measurements using an optical streak camera and spectral measurements using an echelle spectrometer for a laser-produced plasma.

The LPP source was based on the Nd:YAG NL laser system 129-EXPLA and the gas puff target system. The laser system with a wavelength of λ = 1064 nm can provide energy in the range of 1–10 J (3–9 J in this experiment), pulse time duration t = 1 ns or 10 ns (1–2 ns in the short-pulse and 5–10 ns in the long-pulse regime), repetition rate f = 10 Hz, and laser beam diameter = 25 mm (top-hat intensity distribution). The laser beam is focused onto the gas puff target using a plano-convex lens. The resulting intensity reached 10^{14} W/cm^{-2} or 2×10^{13} W/cm^{-2} for short- and long-pulse regimes, respectively. In such conditions, hot plasma is generated directly above the nozzle of the gas valve. The ambient gas filling the chamber is converted to a low-temperature plasma due to exposure to various factors accompanying the LPP formation.

The optical emission of excited molecules and ions that arise in the vicinity of the laser plasma was investigated in a wide spectral range (200–780 nm) using the ESA-4000 echelle spectrometer (LLA Instruments GmbH & Co KG, Berlin, Germany). The spectrometer is equipped with an intensified charge-coupled device (ICCD) camera with a Kodak KAF 1001 detector (spectral resolution of the system was about $\lambda/\Delta\lambda$ ~20 000) [6]. The diameter of the acquisition region is limited by the collecting optical system, approximately 1 mm full width at half maximum (FWHM) in the focal point of the collecting system. The light was acquired at a distance of 6 mm from the LPP. In order to investigate the behavior of the low-temperature plasma, spatial–temporal measurements were carried out. They were made using an optical streak camera (Hamamatsu C10910). The optical axis of the streak camera was perpendicular to the axis of the laser beam, as shown in Fig. 1. Between the entrance slit of the camera and the plasma position, a focusing lens was mounted. It allowed the formation of a plasma image in the plane of the entrance slit. By changing the position of the lens, it was possible to select a narrow observation region at various distances above the LPP.

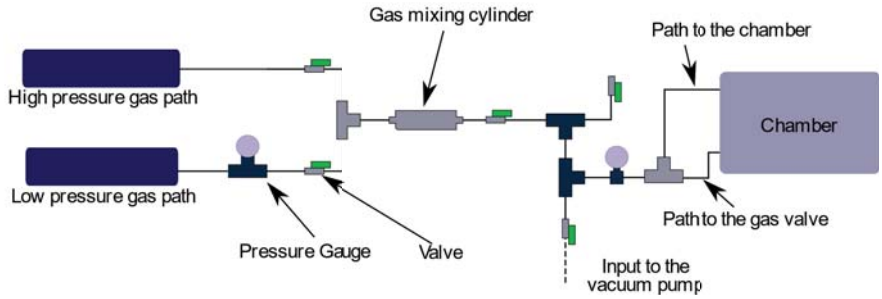

Fig. 2. A special system for mixing noble and molecular gases.

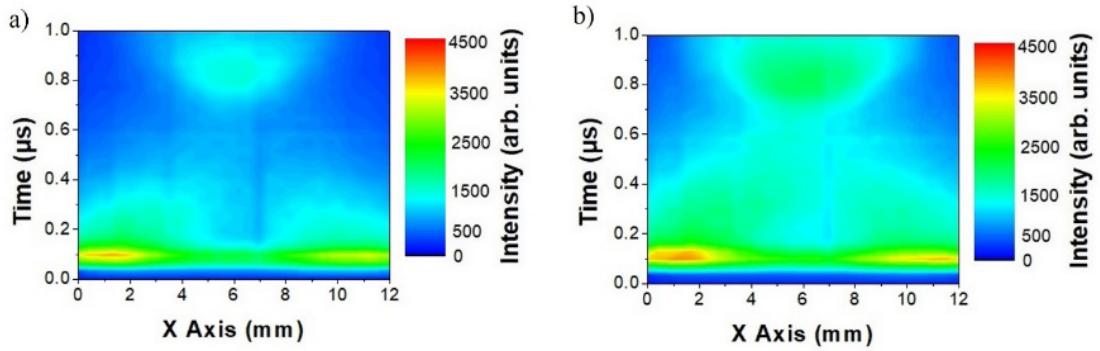

Fig. 3. Spatial–temporal distribution for argon laser-produced plasma. The observation area was 6.6 mm above the LPP source: (a) low-vacuum environment (5×10^{-1} mbar), (b) low argon ambient pressure (~1.3 mbar).

To prepare the gas mixtures, a special system was constructed (Fig. 2), with the aim of creating a mixture to fill the chamber and form the gas puff target. In this work, noble and molecular gases such as Kr, Xe, Ar, He, Ne, H_2, N_2, CO_2, and SF_6 were used to create the mixtures.

Experimental results

Spatial–temporal measurements

Spatial–temporal measurements were made using the optical streak camera for various conditions of low--temperature plasma formation. At first, comparative studies of argon plasmas induced in the vicinity of the LPP, under different conditions, were performed. LPPs were created in the gas puff target, formed in a chamber remaining under a low vacuum (5×10^{-1} mbar) or a low pressure of argon (~1.3 mbar). In our experiments, the term low vacuum means a pressure maintained in the vacuum chamber by a roughing pump. The low pressure was obtained by the controlled injection of a gas into the chamber. The laser was operating in a long-pulse regime with a pulse energy of ~3.9 J. The investigated area was located 6.6 mm above the LPP source. Importantly, the radiation recorded in the streak camera images refers to the EUV/SXR radiation from the laser plasma. The dark area on the *y*-axis (time) is the time needed to synchronize the laser with the triggering of the streak camera. In Fig. 3, the streak images for such parameters are shown. In both cases, the spatial distribution of the optical emission selected by a narrow slit is visible as a function of time. The maximum of the intensity profile taken along the time axis can be noticed after ~80 ns from the beginning of the emission. The corresponding FWHM is ~110 ns. After the next ~700 ns, a second maximum appears with a FWHM of ~250 ns. These parameters are similar in both cases. An important difference concerns the relative intensities for the profiles. The intensities of both maxima recorded for plasmas created under low-vacuum conditions are lower than the corresponding intensities obtained for plasmas induced under low ambient pressure. These maxima are on the same intensity scale.

The influence of pressure on the optical emission of plasmas induced in the ambient gas was also investigated. Measurements were conducted for nitrogen plasmas created in a chamber filled with nitrogen at various pressures: 2.5 mbar, 5 mbar, and 10 mbar (Fig. 4). The observed region, as in the case

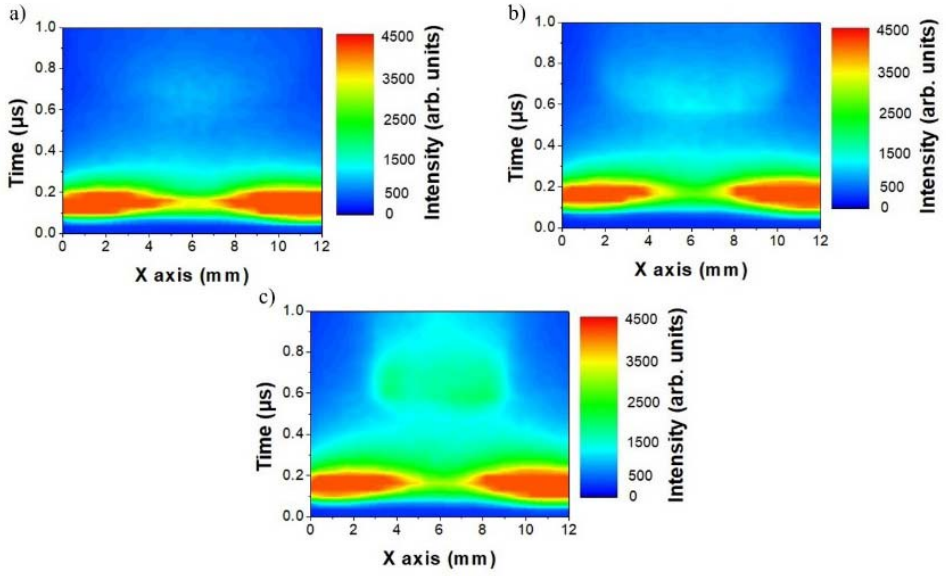

Fig. 4. The spatial–temporal distribution of the intensity obtained from the streak camera for a height of 6.6 mm above the LPP source and at different pressures. The chamber was filled with nitrogen, and the pressure in the chamber was (a) 2.5 mbar, (b) 5 mbar, and (c) 10 mbar.

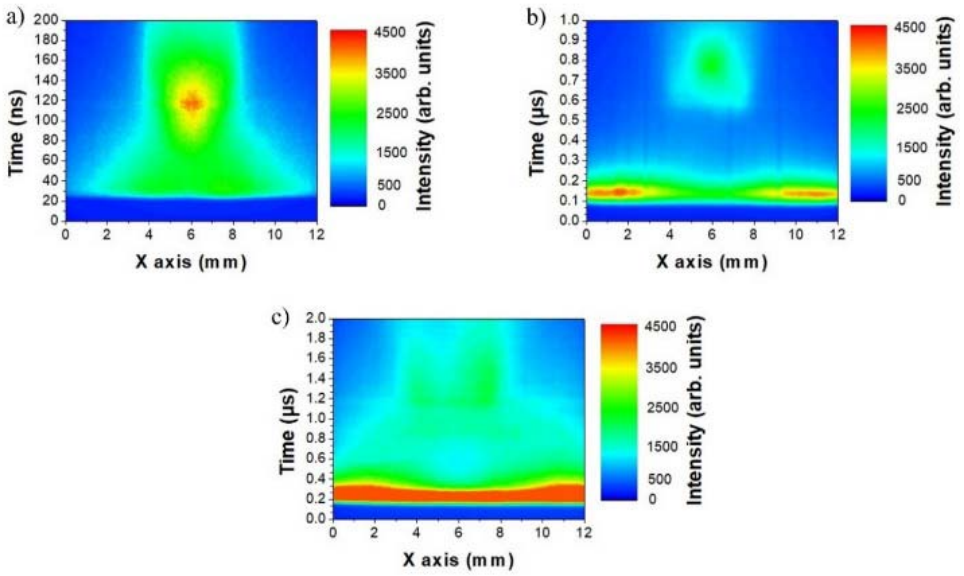

Fig. 5. Spatial–temporal distribution in different time scales and heights: (a) height of 2.8 mm (time scale of 200 ns), (b) 6.6 mm (1 μs), and (c) 8.5 mm (2 μs).

of argon, was 6.6 mm above the LPP source, and the streak camera entrance slit was set at 60 μm. The laser was operating in a short-pulse regime with a pulse energy of ~7.5 J. As can be seen in Fig. 4a, at the ambient pressure of 2.5 mbar, the intensity is strong, but only for the first 250 ns after start of the laser pulse. The same is true under higher pressures, in which case, after this time point, the intensity is still high enough to be seen in the pictures. The FWHM for the regions located 5 mm from the nozzle axis in a horizontal direction (1 mm and 12 mm in the x-axis) for each pressure is about 60 ns and, in the central area, above the nozzle, this is about 120 ns. In addition, the difference between these images is the relative intensity. It concerns especially the second maximum visible at a time point about 600 ns from the beginning of emission. For plasmas created in the ambient gas with a pressure of 10 mbar, it is almost twice as high as that for 2.5 mbar.

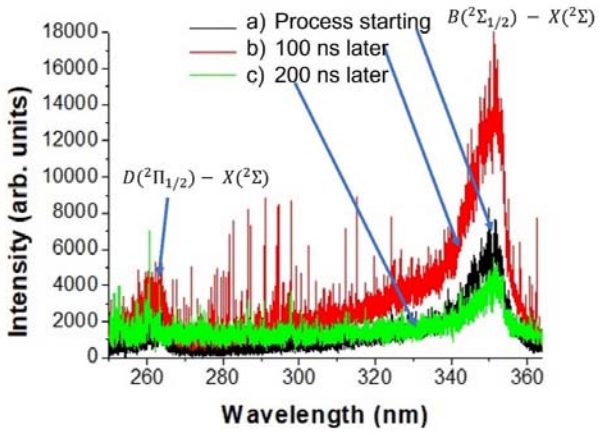

Fig. 6. Spectra from XeF transitions $D(^2\Pi_{1/2}) - X(^2\Sigma)$ and $B(^2\Pi_{1/2}) - X(^2\Sigma)$ area located 6 mm above the LPP source and observed in different moments of the radiation propagation process: (a) start of the process, (b) 100 ns after the start of the process, and (c) 200 ns after the start of the process.

It is also worth looking at how the change of the observation region over the LPP source affects the time–space distribution. Figure 5 shows the streak images recorded for three different distances over the LPP: 2.8 mm, 6.6 mm, and 8.5 mm, respectively. The wider scale makes it possible to observe the formation of high-intensity regions, which widen with distance. In addition, an interesting phenomenon is the occurrence of increased intensity after some time. This is clearly seen in Fig. 5b, at 0.6 μs from the start of the registration process. In Fig. 5c, where the distance from the LPP is the greatest, this intensity area becomes more blurry.

Molecular measurements

The aim of the measurements using the echelle spectrometer was to determine whether it is possible to find molecular spectra in the range of 200–780 nm for the system with the LPP source. The most representative and intense in the studied range were diatomic molecules. Molecular bands expected in this range were carbon compounds and excimers; hence, the prepared mixtures contained selected noble gases CO_2 and N_2 [7–10]. The measurement results presented in Fig. 6 come from the study of the region located 6 mm above the LPP source, and the spectra were observed in different time moments of the low-temperature plasma existence, up to 200 ns after creation of the LPPs. These measurements were performed for a mixture consisting of [2% SF_6, 18% Xe, and 80% He], under the ambient pressure of about 10 mbar and acquisition window of 100 ns. The visible molecular spectra belong to the XeF excimer, and they correspond to the transitions $D(^2\Pi_{1/2}) - X(^2\Sigma)$ and $B(^2\Sigma_{1/2}) - X(^2\Sigma)$ and [8, 9]. The formation process of these molecules is very short, of the order of 200 ns. Investigation has also been carried out in the same conditions, for a mixture of [4% SF_6, 16% Kr, and 80% He]. The KrF excimer

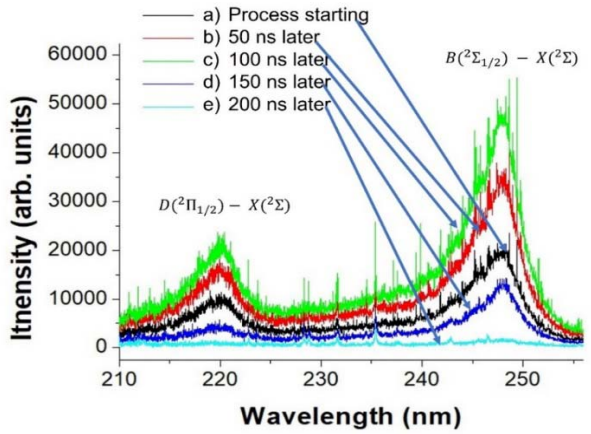

Fig. 7. Spectra from KF transitions $D(^2\Pi_{1/2}) - X(^2\Sigma)$ and $B(^2\Sigma_{1/2}) - X(^2\Sigma)$ for a mixture of gases 2% SF_6, 18% Xe, and 80% He. The investigated region was located 6 mm above the LPP source and observed at differenent moments of the radiation propagation process: (a) start of the process, (b) 50 ns after the start of the process, (c) 100 ns later, (d) 150 ns after the start of the process, and (e) 200 ns after the start of the process.

spectra were obtained and are shown in Fig. 7 [9, 10], with transitions described as $D(^2\Pi_{1/2}) - X(^2\Sigma)$ and $B(^2\Sigma_{1/2}) - X(^2\Sigma)$. The investigated region was located 6 mm above the LPP source and observed for different times of plasma propagation. The formation time of KrF molecules is similar to that for XeF molecules. The formation of some molecules such as excimers is extremely short. The process is of the order of a few/several hundred nanoseconds.

Similar measurements were performed for mixtures containing the molecular gases N_2 and CO_2, at the ambient pressure of about 10 mbar and an acquisition window of 1000 ns. Using such mixtures, apart from the N_2 and CO_2 molecular bands, spectra corresponding to the CN species were also recorded. These spectra, however, were very weak; hence, a Xe admixture was added. In Fig. 8(right), a CN band spectrum recorded for a gas mixture composed of 10% Xe, 10% N_2, and 80% CO_2 is shown.

Discussion of the results

This work is based on the study of low-temperature plasmas induced in gas mixtures. Using various gas mixture parameters, both as an injected mixture and as a mixture filling the chamber, the formation of new molecules, i.e., not constituting the components of the premixture, was observed. This experiment showed that the LPP source is able to provide conditions for the formation of molecules and their registration using spectral methods.

Based on the pictures presented in Fig. 3, it can be concluded that the propagation of radiation from the LPP source depends on the conditions in the chamber. Low vacuum causes fewer instances of photoionization and ionization than does a chamber filled with gas under low pressure. It is worth noting that in the images from the streak camera in the area close to and above the nozzle, we observe a visibly lower intensity than in the diagonal direction. This is due to the fact that the SXR radiation is strongly absorbed near the LPP source; therefore, it can hardly propagate in the gas injection path. On the other hand, at the border of the injected gas with the ambient gas, this radiation can propagate and ionize the gas. The resulting low-temperature plasma emits light, which is visible as intense maxima on the right and left sides of the streak images [11]. Optical radiation recorded for the central area above the LPP, occurring at a time point of approximately 600 ns (Figs. 4 and 5), cannot be induced by the EUV/SXR radiation. At this time point, the hot and dense plasma emitting the energetic photons does not exist. The emission maximum recorded after such a long time could be a result of the propagation of the shockwave or the formation of low-temperature plasma by the fast ions or electrons from the LPP. A detailed analysis concerning occurrence of this emission maximum supported by the corresponding numerical simulations was reported by Bartnik *et al*. [11].

Apart from spatial–temporal measurements, spectral measurements in the optical range were also performed. Contrary to the atomic spectra, molecular ones are composed of bands, corresponding to molecular electronic transitions. Such spectra can be simulated using one of the available numerical codes, e.g., PGOPHER [12]. To perform the simulations for a specific molecule, the necessary vibration and rotational constants have to be applied. Due to the fact that real molecules have anharmonic potentials, the energies of the vibration levels have to be calculated based on Eq. (1).

$$E(v) = T_e + \omega_e(v + \tfrac{1}{2}) - \omega_e x_e(v + \tfrac{1}{2})^2 + \omega_e y_e\,(v + \tfrac{1}{2})^3 + \ldots, \tag{1}$$

where v is the vibrational quantum number, T_e is the minimum electronic energy (in inverse centimeters [cm^{-1}]), ω_e is the first vibrational term (cm^{-1}), $\omega_e x_e$ is the second vibrational term (cm^{-1}), and $\omega_e y_e$ is the third vibrational term (cm^{-1}). If we consider a molecule with an anharmonic potential, the rotational constant changes slightly with the vibrational state. The rotational constant B_v for a given vibrational state can be described by the expression in Eq. (2).

$$B_v\, B_e - \alpha_e(v + \tfrac{1}{2}) + \gamma_e(v + \tfrac{1}{2})^2 + \ldots, \tag{2}$$

where B_e is the rotational constant in equilibrium position (cm^{-1}), α_e is the first rotational term (cm^{-1}), and γ_e is the rotation–vibration interaction constant (cm^{-1}).

The necessary molecular constants can be found in the database of the National Institute of Standards and Technology (NIST) [13].

The simulation results for CN molecules were compared with the spectral observations using a mixture of [10% Xe, 10% N_2, and 80% CO_2] and are shown in Fig. 8. Transitions for the selected spectra come from the states $B^2\Sigma^+ - X^2\Sigma^+$. As you can see, the simulations reflect the nature of the observations quite well. The process of formation of CN

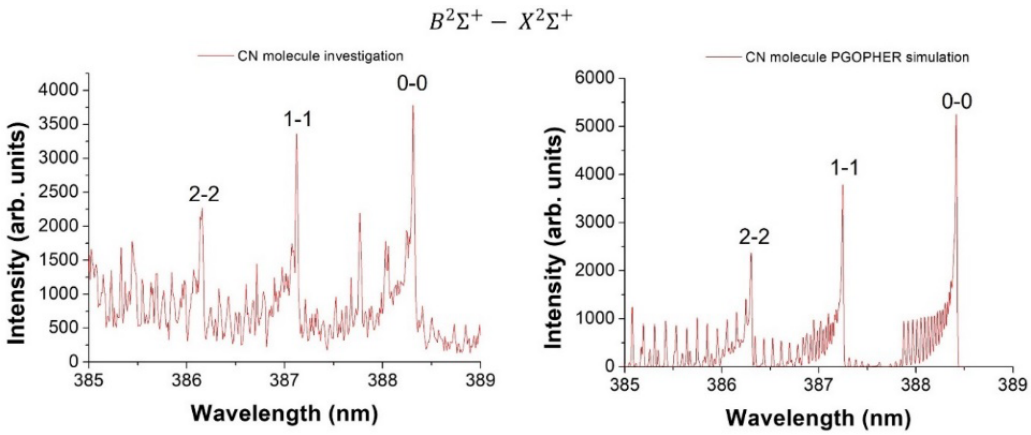

Fig. 8. Comparison of the spectrum obtained from the simulation in the PGOPHER program (right) with the measurement made with the echelle spectrometer for the states (left) for CN molecules.

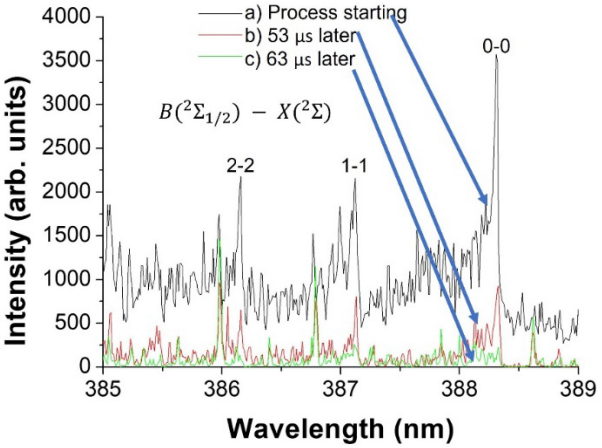

Fig. 9. Spectra showing the duration of the formation processes of the CN molecule: (a) start of the process, (b) 53 μs later, and (c) 63 μs later.

molecules is much longer than that of the excimer molecules – compare Figs. 8 and 9. Their formation lasts for tens of microseconds.

Summary

In this work, emission of LPP formed in low-pressure ambient gas from the gas puff target was studied. As part of this work, the research was divided into methods that used streak cameras for spatial–temporal measurements and methods using spectroscopic measurements of molecular spectra. The analysis of images from the streak camera allowed us to examine the nature of radiation emission and the regions where the expected emission is the highest. This, in turn, contributed to the registration of molecular spectra, along with their subsequent analysis and simulations in numerical programs. The excimers found showed interesting spectra; the time in which they were created was a few/several hundred nanoseconds. These studies provide the basis for further molecular analyses in such a system, as well as premises for analyses in wider spectral ranges, e.g., in the infrared region.

Acknowledgment. This work was supported by the National Science Centre, Poland, under grant agreement no. 2020/39/B/ST2/00509.

ORCID

A. Bartnik http://orcid.org/0000-0002-7555-8426
H. Fiedorowicz http://orcid.org/0000-0002-7022-3408
T. Fok http://orcid.org/0000-0001-9583-0389
M. Majszyk http://orcid.org/0000-0002-8665-4309
W. Skrzeczanowski http://orcid.org/0000-0003-2727-9833
M. Szczurek http://orcid.org/0000-0002-8794-2118
Ł. Węgrzyński http://orcid.org/0000-0002-1532-0459

References

1. Hu, R., Seager, S., & Bains, W. (2012). Photochemistry in terrestrial exoplanet atmospheres I: Photochemistry model and benchmark cases. *Astrophys. J.*, *761*(2), 166. DOI: 10.1088/0004-637X/761/2/166.
2. Rimme, P. B., Ferus, M., & Waldmann, I. P. (2019). Identifiable acetylene features predicted for young Earth-like exoplanets with reducing atmospheres undergoing heavy bombardment. *Astrophys. J.*, *888*(1), 21. DOI: 10.3847/1538-4357/ab55e8.
3. Dobrijevic, M., & Parisot, J. P. (1995). Numerical simulation of organic compounds formation in planetary atmospheres: Comparison with laboratory experiments. *Adv. Space Res.*, *15*(10), 1–4. DOI: 10.1016/0273-1177(94)00143-O.
4. Löhle, S., Zander, F., & Hermann, T. A. (2017). Experimental simulation of meteorite ablation during Earth entry using a plasma wind tunnel. *Astrophys. J.*, *837*(2), 170–178. DOI: 10.3847/1538-4357/aa5cb5.
5. Bartnik, A., Skrzeczanowski, W., & Wachulak, P. (2021). Spectral investigations of low-temperature plasma induced in CO2 gas by nanosecond pulses of extreme ultraviolet (EUV). *Plasma Sources Sci. Technol.*, *30*(11), 115008. DOI: 10.1088/1361-6595/ac2e9a.
6. Skrzeczanowski, W., & Długaszek, M. (2021). Al and Si quantitative analysis in aqueous solutions by LIBS method. *Talanta*, *225*, 121916. DOI: 10.1016/j.talanta.2020.121916.

7. Tellinghuisen, P. C., Tellinghuisen, J., & Tisone, G. C. (1978). Spectroscopic studies of diatomic noble gas halides. III. Analysis of XeF 3500 Å band system. *J. Chem. Phys.*, *68*(11), 5187–5198. DOI: 10.1063/1.435582.
8. Tellinghuisen, P. C., Tellinghuisen, J., & Coxon, J. A. (1978). Spectroscopic studies of diatomic noble gas halides. IV. Vibrational and rotational constants for the X, B, and D states of XeF. *J. Chem. Phys.*, *68*(11), 5177–5186. DOI: 10.1063/1.435583.
9. Tellinghuisen, J., Hays, A. K., & Hoffman, J. M. (1976). Spectroscopic studies of diatomic noble gas halides. II. Analysis of bound-free emission from XeBr, XeI, and KrF. *J. Chem. Phys.*, *65*(11), 4473–4482. DOI: 10.1063/1.432994.
10. Huber, K. P., & Herzberg, G. (1979). *Molecular spectra and molecular structure, IV. Constants of diatomic molecules*. New York: Springer.
11. Bartnik, A., Jach, K., & Świerczyński, R. (2022). Dynamics of plasmas produced by a laser pulse, inside a dense gaseous target, formed in an ambient gas. *Phys. Plasmas*, *29*(9), 093302. DOI: 10.1063/5.0099683.
12. Western, C. M. (2016). PGOPHER: A program for simulating rotational, vibrational and electronic spectra. *J. Quant. Spectrosc. Radiat. Transf.*, *186*, 221–242. DOI: 10.1016/j.jqsrt.2016.04.010.
13. National Institute of Standards and Technology. (2021). *The Digital Millennium Copyright Act (DMCA)*. Updated October 1, 2021, from https://webbook.nist.gov/chemistry.